Hingeless Helicopter Rotor Response with Nonuniform Inflow and Elastic Blade Bending

ROBERT A. ORMISTON* AND DAVID A. PETERS†
U.S. Army Air Mobility R & D Laboratory, Moffett Field, Calif.

A generalized harmonic balance theory for the steady-state, linear, response characteristics of a hingeless rotor in forward flight is presented and evaluated with the aid of recent experimental data. Comparisons of several approximate representations for the rotor blade revealed that the simple rigid hinged blade is inadequate except at very low advance ratios, or high flap frequencies. For typical values of flap frequency the first two elastic flap bending modes are required for accurate response predictions. Simplified models of the nonuniform induced inflow were derived, using momentum and vortex theory, and found to be the most important factor in improving correlation with the data. An empirical inflow model was developed from the experimental data by obtaining an inverse solution of the present theory. This inflow model was found to be in reasonable agreement with the simple inflow theories for low advance ratios but revealed large unexpected variations in the induced inflow of the rotor for advance ratios near 0.8.

Nomenclature

a = two-dimensional lift curve slope, rad^{-1}
B = tip loss factor
b = number of blades
c = blade chord, ft
C_T = thrust coefficient, thrust/$\rho\pi\Omega^2R^4$
C_l = roll moment coefficient, roll moment/$\rho\pi\Omega^2R^5$
C_m = pitch moment coefficient, pitch moment/$\rho\pi\Omega^2R^5$
e = dimensionless radial flapping hinge offset for rigid blade
e_{pc} = rotor blade pocket cutout, dimensionless radius of ineffective blade area
EI = rotor blade bending stiffness
$\{dF\}$ = generalized rotor thrust and moments
J = number of flap bending modes
$[L]$ = nonuniform induced inflow matrix
m = rotor blade mass distribution, slug/ft
$[M]$ = rotor response partial derivative matrix for control inputs without inflow
$[N]$ = rotor response partial derivative matrix for induced inflow components
n = number of azimuthal harmonics
p = nondimensional fundamental rotor blade flap frequency, $p = \omega/\Omega$
r = rotor blade radial coordinate, ft
R = rotor blade radius, ft
U_∞ = freestream velocity, fps
v_i = induced inflow velocity, fps
v_o = mean induced velocity, fps
w = rotor blade flap deflection, ft
γ = Lock number, $\rho acR^4/\int_0^R r^2 dm$
γ^* = equivalent Lock number, Eq. (25)
$\{d\theta\}$ = generalized control inputs
θ = rotor blade pitch angle, rad
$\theta_o,\theta_s,\theta_c$ = collective and cyclic pitch, rad
$\{d\lambda\}$ = generalized inflow components
λ_i = nondimensional induced velocity, $\lambda_i = v_i/R\Omega$
$\lambda_o,\lambda_s,\lambda_c$ = uniform and nonuniform induced velocity components
μ = advance ratio, $U_\infty/R\Omega$
ρ = air density, slugs/ft^3
σ = rotor solidity, $bc/\pi R$
τ = nondimensional time, $\tau = \Omega t = \psi$
ψ = rotor blade azimuth position, rad
Ω = rotor blade angular velocity, rad/sec
ω = rotor blade flap frequency, rad/sec

Superscripts
$(\,)'$ = $\partial/\partial r$
$(\dot{})$ = $\partial/\partial\tau$

Presented as Paper 72-65 at the AIAA 10th Aerospace Sciences Meeting, San Diego, Calif., January 17–19, 1972; submitted January 27, 1972; revision received April 28, 1972.
Index category: Rotary Wing and VTOL Aerodynamics.
* Research Scientist, Ames Directorate. Member AIAA.
† Research Scientist, Ames Directorate. Student Member AIAA.

Introduction

THE unique feature of hingeless rotors is the absence of rotor blade flapping and lead-lag hinges found on conventional articulated rotor helicopters. The cantilevered blades can thus apply bending moments to the rotor hub, substantially increasing the vehicle control power and damping and improving maneuverability and flying qualities.

The steady-state rotor moments and thrust generated by control inputs, i.e., the rotor response characteristics, are therefore important basic properties of hingeless rotors. Nevertheless, considerable uncertainty exists regarding the importance of nonuniform induced inflow and higher mode, elastic blade bending deflections in the prediction of these response characteristics. The nonuniform inflow is a direct result of the large hub moments developed by hingeless rotors. Interestingly, neither the induced inflow nor elastic blade bending are of comparable importance for articulated rotor response.

The simplest method for predicting hingeless rotor response employs a spring restrained, centrally hinged, rigid blade to approximate the flapping deflections of the actual cantilevered elastic blade. This model, including reversed flow effects on the retreating blades, but not induced inflow, was used by Sissingh[1] to predict rotor response at high advance ratios, and was recently correlated with wind-tunnel measurements of a 7.5 ft model at the Ames Directorate, USAAMRDL.[2] The qualitative response characteristics were reasonably well predicted by the theory, but significant discrepancies were present, especially in hover and at low advance ratio. A similar theory[3] using an approximate mode shape for the first flap mode was correlated with wind-tunnel data for a 33′ hingeless rotor, yielding similar results.

A more elaborate theory by Shupe,[4] including the first two elastic flap bending modes, and a simplified representation of nonuniform inflow based on momentum theory indicated that both the second flap bending mode and the inflow could significantly influence hingeless rotor response. These important results were not substantiated in detail, however, and were restricted to low advance ratios because reversed flow effects were not included.

The evident lack of full understanding of these factors and their important relationship to the fundamental response characteristics of hingeless rotors led to the present investigation. A comprehensive theory is used to examine analytically the relative importance of various flap bending modes and mode shapes, and to evaluate several simplified models of nonuniform induced inflow. The theory is also evaluated by comparison with experimentally measured data from both small and large scale hingeless rotors.

Generalized Harmonic Balance Method for Hingeless Rotor Blades

This technique is a generalization of the simple harmonic balance methods which have long been used to predict articulated rotor response, except that an arbitrary number of elastic bending modes, and azimuthal harmonics for the amplitude of each mode are included, in addition to a rational treatment of reversed flow aerodynamics.

We begin with the linear equation of motion for the deflection of an elastic beam[5] subject to a distributed aerodynamic load F, (lb/ft), written in the rotating coordinate system,

$$(EIw'')'' + m\Omega^2\ddot{w} + \Omega^2[mrw' - w''\int_r^R mrdr] = F(r,\psi) \quad (1)$$

The associated expressions for bending moment and shear at the blade root are

$$M(0,\tau) = \int_o^R [F - m\Omega^2(\ddot{w} + w)]rdr \quad (2)$$

$$V(0,\tau) = \int_o^R [F - m\Omega^2\ddot{w}]dr \quad (3)$$

The blade root bending moment is transformed into a stationary coordinate system, to yield the pitch and roll moment of the rotor. The ultimate solution of Eq. (1) yields the blade deflections, and together with Eqs. (2) and (3) the rotor thrust and moments which are the desired response parameters. Assuming an approximate expression for the blade deflection in terms of elastic bending modes $\phi_j(r)$,

$$\frac{w}{R} = \sum_{j=1}^{J} q_j(\tau)\phi_j(r) \quad (4)$$

For the present analysis, the modal functions $\phi_j(r)$ were approximated by the common bending modes for a uniform nonrotating cantilever beam which are available in Ref. 5. The nonrotating modes are a reasonable approximation for rotating beam modes which can be found in Ref. 6.

The bending mode amplitudes are expressed in a Fourier series in terms of nondimensional time or equivalently the rotor blade azimuthal position ψ. This series is truncated at the highest azimuthal harmonic of interest N. In general, for an arbitrary number J of elastic modes there will be N harmonics for each mode.

$$q_j(\tau) = a_{j0} + \sum_{n=1}^{N} (a_{jn}\cos n\psi + b_{jn}\sin n\psi) \quad (5)$$

The aerodynamic loading may be expressed in terms of harmonics of the blade bending mode amplitudes (a_{jn}, b_{jn}) and the blade mode shapes ϕ_j. Galerkin's method is then used to reduce the partial differential equation, Eq. (1), to J ordinary differential equations in terms of q_j. Substitution of the assumed Fourier series for q_j, Eq. (5), gives an equation in terms of each of the sine and cosine harmonics present. The coefficients of these harmonics, which are linear combinations of the bending mode harmonic amplitudes (a_{jn}, b_{jn}), are set equal to zero giving $(2N+1)J$ linear algebraic equations in terms of a_{jn}, b_{jn}. Finally, these may be used in Eqs. (2) and (3) to yield the rotor thrust and moment response characteristics.

Aerodynamic Loading

Since the basic equations for the aerodynamic load distribution are available in the literature[1] only a brief description of their derivation will be given. The lift per unit span may be written as

$$F = s(\rho ac/2)(U_T^2\theta - U_P U_T) \quad (6)$$

The parameter s accounts for the sign reversal of F in the reversed flow region, and $s = \pm 1$ when $r/R \gtrless -\mu\sin\psi$. The velocity components U_T and U_P are given by

$$U_T/R\Omega = r/R + \mu\sin\psi \quad (7)$$

$$U_P/R\Omega = \dot{w}/R + \lambda_i + \mu w'\cos\psi \quad (8)$$

It is here that the effects of induced inflow and elastic blade bending are directly evident. Both the deflection and slope of the blade contribute to the perpendicular velocity component U_P. In general the induced inflow is a function of radius and azimuth, $\lambda_i = \lambda_i(r,\psi)$, but only the azimuthal nonuniformity will be retained. Furthermore λ_i will be approximated by a truncated Fourier series

$$\lambda_i = \lambda_o + \lambda_s\sin\psi + \lambda_c\cos\psi \quad (9)$$

The usual uniform inflow of classical rotor aerodynamics is represented by λ_o, while the nonuniform inflow treated in this paper is embodied in λ_s and λ_c. The rotor blade pitch angle θ is given by the usual equation for collective, longitudinal cyclic, and lateral cyclic pitch

$$\theta = \theta_o + \theta_s\sin\psi + \theta_c\cos\psi \quad (10)$$

When these equations are combined and integrated using Galerkin's method the resulting areodynamic loading becomes a linear combination of the independent parameters of the problem. If the integrated loading is denoted by $\bar{F}$ this implies

$$\bar{F} = \bar{F}(\theta_o,\theta_s,\theta_c\lambda_o,\lambda_s,\lambda_c) \quad (11)$$

Each of these parameters may be considered control inputs or forcing functions of the aerodynamic loading. The constant of proportionality for each control input is nonanalytic because of the reversed flow region but can be represented by a Fourier series in ψ. Furthermore, the coefficients of each Fourier harmonic are functions of the blade bending mode shapes and their derivatives, ϕ_j, ϕ_j', the advance ratio μ, the tip loss factor B, and pocket cutout e_{pc}.

Results of Generalized Harmonic Balance Method

The results obtained from the generalized harmonic balance method include the N azimuthal harmonics of the rotor blade deflection for each of the J bending modes. The harmonics of rotor thrust, pitch moment, and roll moment which result from summation of the contributions of all bending modes in Eqs. (2) and (3) are also obtained. For the present purposes only the steady-state components of the thrust and moment response for each of the control input parameters are relevant. Since these response components are actually partial derivatives with respect to the various control inputs, the total differentials of the thrust and moments can be written concisely in matrix notation as follows:

$$\begin{Bmatrix} d\frac{C_T}{a\sigma} \\ d\frac{C_l}{a\sigma} \\ d\frac{C_m}{a\sigma} \end{Bmatrix} = \begin{bmatrix} \frac{\partial(C_T/a\sigma)}{\partial\theta_o} & \frac{\partial(C_T/a\sigma)}{\partial\theta_s} & \frac{\partial(C_T/a\sigma)}{\partial\theta_c} \\ \frac{\partial(C_l/a\sigma)}{\partial\theta_o} & \frac{\partial(C_l/a\sigma)}{\partial\theta_s} & \frac{\partial(C_l/a\sigma)}{\partial\theta_c} \\ \frac{\partial(C_m/a\sigma)}{\partial\theta_o} & \frac{\partial(C_m/a\sigma)}{\partial\theta_s} & \frac{\partial(C_m/a\sigma)}{\partial\theta_c} \end{bmatrix} \begin{Bmatrix} d\theta_o \\ d\theta_s \\ d\theta_c \end{Bmatrix} + \begin{bmatrix} \frac{\partial(C_T/a\sigma)}{\partial\lambda_o} & \frac{\partial(C_T/a\sigma)}{\partial\lambda_s} & \frac{\partial(C_T/a\sigma)}{\partial\lambda_c} \\ \frac{\partial(C_l/a\sigma)}{\partial\lambda_o} & \frac{\partial(C_l/a\sigma)}{\partial\lambda_s} & \frac{\partial(C_l/a\sigma)}{\partial\lambda_c} \\ \frac{\partial(C_m/a\sigma)}{\partial\lambda_o} & \frac{\partial(C_m/a\sigma)}{\partial\lambda_s} & \frac{\partial(C_m/a\sigma)}{\partial\lambda_c} \end{bmatrix} \begin{Bmatrix} d\lambda_o \\ d\lambda_s \\ d\lambda_c \end{Bmatrix} \quad (12)$$

The separate grouping of the response derivatives emphasizes the difference between the actual physical control inputs $(\theta_o,\theta_s,\theta_c)$ and the "inputs" due to the three induced inflow components $(\lambda_o,\lambda_s,\lambda_c)$.

Induced Inflow Theory

The important role of induced inflow for the solution of the rotor response problem is illustrated by Eq. (12). The physical control inputs are considered independent parameters while the inflow components are dependent variables related to the thrust and moments produced by the rotor. The complete solution for the rotor response derivatives is obtained only when the inflow components do not appear explicitly in Eq. (12). This can be accomplished quite simply if the following linear relationship between the inflow components and the rotor thrust and moments is postulated:

$$\begin{Bmatrix} d\lambda_o \\ d\lambda_s \\ d\lambda_c \end{Bmatrix} = \begin{bmatrix} \frac{d\lambda_o}{d(C_T/a\sigma)} & \frac{d\lambda_o}{d(C_l/a\sigma)} & \frac{d\lambda_o}{d(C_m/a\sigma)} \\ \frac{d\lambda_s}{d(C_T/a\sigma)} & \frac{d\lambda_s}{d(C_l/a\sigma)} & \frac{d\lambda_s}{d(C_m/a\sigma)} \\ \frac{d\lambda_c}{d(C_T/a\sigma)} & \frac{d\lambda_c}{d(C_l/a\sigma)} & \frac{d\lambda_c}{d(C_m/a\sigma)} \end{bmatrix} \begin{Bmatrix} d\frac{C_T}{a\sigma} \\ d\frac{C_l}{a\sigma} \\ d\frac{C_m}{a\sigma} \end{Bmatrix} \quad (13)$$

Equations (12) and (13) may be written as follows:

$$\{dF\} = [M]\{d\theta\} + [N]\{d\lambda\} \quad (14)$$

$$\{d\lambda\} = [L]\{dF\} \quad (15)$$

Now $\{dF\}$, $\{d\theta\}$, and $\{d\lambda\}$ are vectors representing the generalized rotor forces, control parameters, and inflow components respectively. The general nonuniform inflow model is denoted by the matrix $[L]$ while $[M]$ and $[N]$ are the rotor response partial derivatives from the generalized harmonic balance method. Simultaneous solution of these equations yields the desired relation for the generalized rotor response forces

$$\{dF\} = [M']\{d\theta\} \quad (16)$$

where

$$[M'] = [I - [N][L]]^{-1}[M] \quad (17)$$

Here the matrix $[M']$ is composed of the rotor response partial derivatives including the effects of nonuniform induced inflow. A comparison of $[M]$ and $[M']$ would directly reveal the magnitude of the inflow contribution to the rotor response characteristics.

While no rigorous theoretical justification exists for the form of the inflow-force relation embodied in Eq. (13) it does represent a convenient formulation for use with the harmonic balance method, and can easily accommodate a variety of simple approximations, based on momentum or vortex theory, for the various inflow derivatives. Furthermore, it has the advantage of permitting the solution of an inverse problem, i.e., determining the inflow components indirectly from experimental data.

Inverse Problem

With the present formulation of the induced inflow theory it is a simple matter to solve the inverse problem for the inflow matrix $[L]$ itself. Given experimental measurements for the rotor response derivatives $[M']$ and the response partial derivatives for the control inputs and inflow components $[M]$ and $[N]$, respectively, from the generalized harmonic balance method, Eq. (17) can be used to obtain an empirical estimate for the inflow matrix $[L]$

$$[L] = [N]^{-1}[I - [M][M']^{-1}] \quad (18)$$

Nonuniform Induced Inflow Models

Since the inflow model postulated by Eq. (13) is only an approximation for the highly complex induced velocity field of a rotor it is consistent to use simplified methods to estimate the individual inflow derivatives.

The first method employs classical rotor momentum theory[7] applicable to forward flight conditions. The differential force on an elemental area of the rotor disc is given by $dF = 2v_i\, d\dot{m}$ where $2v_i$ is the total change in velocity normal to the disc. The differential mass flow through the element is based on the resultant vector velocity at the element

$$d\dot{m} = \rho|\mathbf{V}|rdrd\psi \quad (19)$$

For the case of freestream velocity parallel to the rotor disc and negligible mean inflow (nonlifting rotor condition) the resultant velocity is $|\mathbf{V}| \simeq U_\infty$. In the hover condition at high thrust (high mean inflow, v_o) the resultant velocity is $|\mathbf{V}| \simeq v_o$. When these equations are combined with Eq. (9) and integrated over the rotor disk, linearized expressions for the thrust and moment are obtained in terms of the inflow components λ_o, λ_s, λ_c. The inflow model $[L]$ then becomes, for the hover condition

$$\begin{Bmatrix} d\lambda_o \\ d\lambda_s \\ d\lambda_c \end{Bmatrix} = \frac{a\sigma}{\lambda_o} \begin{bmatrix} \frac{1}{4} & 0 & 0 \\ 0 & -\frac{3}{4} & 0 \\ 0 & 0 & -\frac{3}{4} \end{bmatrix} \begin{Bmatrix} dC_T/a\sigma \\ dC_l/a\sigma \\ dC_m/a\sigma \end{Bmatrix} \quad (20)$$

and for the forward flight condition

$$\begin{Bmatrix} d\lambda_o \\ d\lambda_s \\ d\lambda_c \end{Bmatrix} = \frac{a\sigma}{\mu} \begin{bmatrix} \frac{1}{2} & 0 & 0 \\ 0 & -\frac{3}{2} & 0 \\ 0 & 0 & -\frac{3}{2} \end{bmatrix} \begin{Bmatrix} dC_T/a\sigma \\ dC_l/a\sigma \\ dC_m/a\sigma \end{Bmatrix} \quad (21)$$

A second method for deriving an inflow model, amenable to the forward flight condition, is based on simple vortex systems arranged to produce the desired forces and moments. Consider the rotor to be represented by a simple horseshoe vortex system consisting of a bound vortex of circulation Γ at the lateral axis with two trailing vortices extending rearward in the plane of rotation. This vortex system will produce a longitudinal gradient of induced velocity at the center of the rotor. Accounting for both the bound and trailing vortices the gradient is approximately

$$dv_i/dr \cong \Gamma/\pi R^2 \quad (22)$$

The longitudinal gradient is also related to the cosine component of the induced velocity, $v_c = \Gamma/\pi R$. Furthermore the rotor thrust is given by $T = 2\rho U_\infty \Gamma R$. These equations can be combined and nondimensionalized to yield,

$$\lambda_c = C_T/2\mu \quad (23)$$

Similar relations can be developed for the inflow derivatives $d\lambda_o/d(C_T/a\sigma)$ and $d\lambda_s/d(C_l/a\sigma)$ with proper choice of the vortex geometry. Such results very nearly match the momentum theory; hence they will not be detailed here. An exception

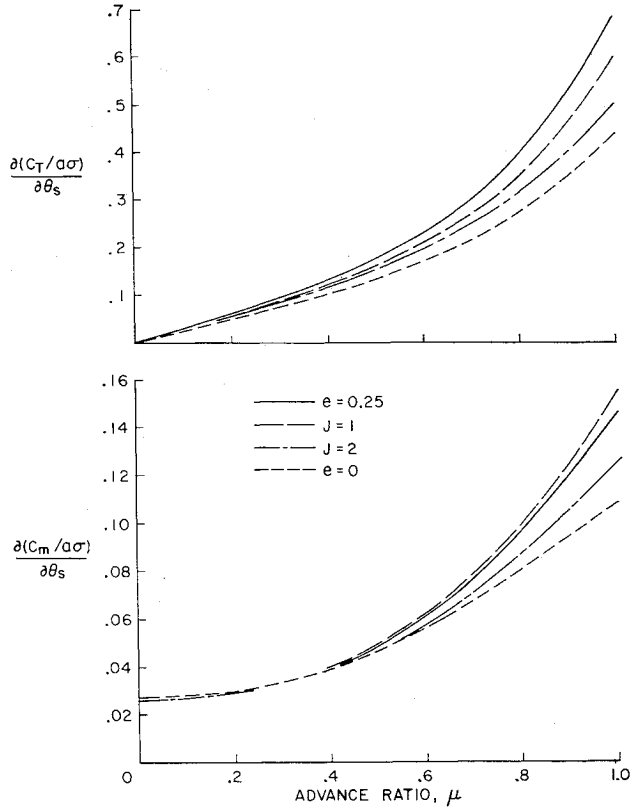

Fig. 1 Effect of elastic bending modes and hinge offset on rotor response partial derivatives without induced inflow, $p = 1.2$, $\gamma = 5.0$, $B = 0.97$, $e_{pc} = 0.0$.

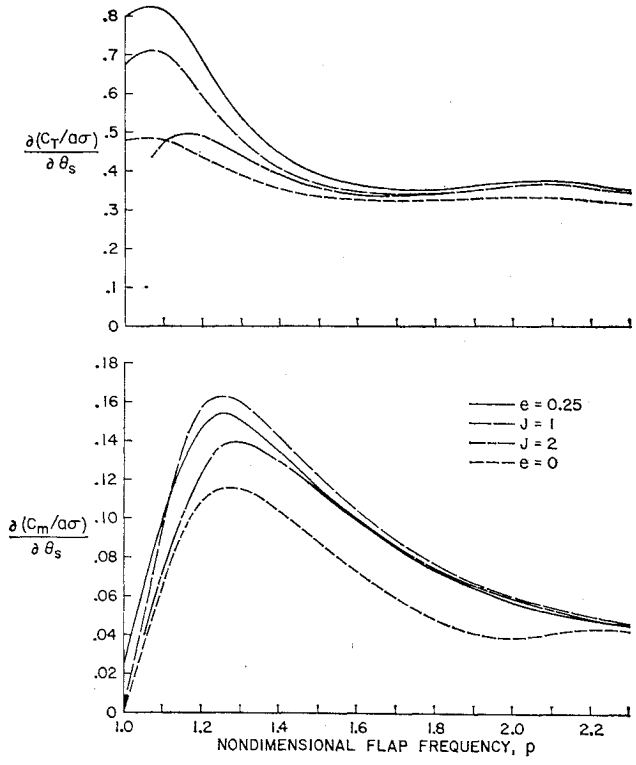

Fig. 2 Effect of elastic bending modes and hinge offset on rotor response partial derivatives without induced inflow, $\mu = 1.0$, $\gamma = 5.0$, $B = 0.97$, $e_{pc} = 0.0$.

is that the vortex modeling does not predict a $d\lambda_c/d(C_m/a\sigma)$ inflow derivative. An inflow model based on vortex theory then becomes

$$\begin{Bmatrix} d\lambda_o \\ d\lambda_s \\ d\lambda_c \end{Bmatrix} = \frac{a\sigma}{\mu} \begin{bmatrix} \frac{1}{2} & 0 & 0 \\ 0 & 7-\frac{3}{2} & 0 \\ \frac{1}{2} & 0 & 0 \end{bmatrix} \begin{Bmatrix} dC_T/a\sigma \\ dC_l/a\sigma \\ dC_m/a\sigma \end{Bmatrix} \tag{24}$$

These simple theoretical inflow models lend themselves to physical interpretation of the character of the induced inflow of a rotor. Especially in the case of the momentum theory it is evident that forces distributed around the rotor azimuth accelerate the air stream at those points, producing a similar distribution of induced velocity. In essence the air stream yields in response to forces applied to it. Furthermore the resulting induced velocities are inversely proportional to the mean inflow λ_o in hover and the advance ratio μ in forward flight. Therefore, the higher the thrust or forward velocity in hover or forward flight, respectively, the lower the incremental induced velocities.

Theoretical Results

The generalized harmonic balance method was used to investigate the effects of the number of flap bending modes and mode shape on two representative rotor response partial derivatives. The simplest model is the spring restrained, centrally hinged ($e = 0$) rigid blade. A more accurate rigid blade model incorporates an offset flapping hinge ($e = 0.25$) and gives a closer approximation to the shape of the actual first elastic flap mode. Two cases using the elastic blade bending modes were examined, with a single first flap mode ($J = 1$) and with the first and second flap modes ($J = 2$), respectively. The results for these four configurations are shown in Figs. 1 and 2. At low advance ratios, the elastic bending effects are negligible and the simple rigid blade representation is quite accurate. At moderately high advance ratios, considerable differences arise. Figure 2, for $\mu = 1.0$, illustrates that these differences are highly dependent on the nondimensional rotating flap frequency p. For very stiff blades, (large p) the simple rigid blade representations are adequate but for flexible blades, typical of hingeless rotors ($p \sim 1.15$) the more exact modal representations are required. In particular, the second flap bending mode is important for accurate response predictions.

To illustrate the main effects of nonuniform inflow, Eq. (17) was used to predict the response derivatives in Fig. 3 using the momentum theory inflow model. Because of the inverse relationship of induced inflow with advance ratio, the large reduction in control power $d(C_m/a\sigma)/d\theta_s$ at low μ is not surprising. For the momentum theory the inflow derivative matrix, Eq. (24), is diagonal and all nine response derivatives vanish in the limit as μ approaches zero. Since the simple inflow theories were derived for zero rotor lift in forward flight, they are valid only for zero mean inflow, λ_o. For the lifting rotor condition, however, Eq. (24) would be dependent on λ_o and not all of the response derivatives would vanish for $\mu = 0$.

It is significant to point out that the inverse relationship of inflow with advance ratio can be intuitively misleading. Many researchers have neglected the effects of induced inflow at high advance ratio on this basis. The results in Fig. 3, however, show this assumption to be incorrect. For $d(C_m/a\sigma)/d\theta_s$ the effects of inflow at low advance ratio do diminish with increasing μ, but only up to a point. Beyond that, the rotor response becomes increasingly sensitive to the effects of inflow. For $d(C_T/a\sigma)/d\theta_s$, the effect of inflow increases continuously with μ for the entire advance ratio range.

Comparison of Theory and Experimental Data

The principle experimental data to be used in the following correlations was obtained with 7.5 ft hingeless rotor model

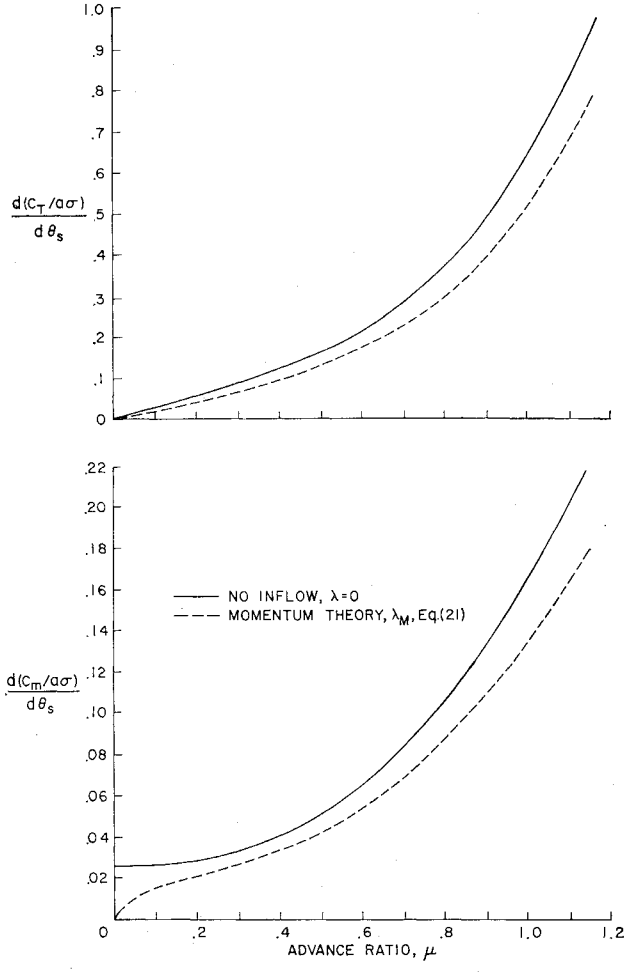

Fig. 3 Effect of nonuniform induced inflow on rotor response derivatives, $C_T/\sigma = 0.0$, $p = 1.2$, $\gamma = 5.0$, $B = 0.97$, $e_{pc} = 0.0$, $a\sigma = 0.729$, $J = 1$.

tested in the USAAMRDL-Ames wind tunnel.[2,8] The model configuration and test conditions varied over a wide parameter range, including flap frequencies from $p = 1.17$ to 2.32 and advance ratios from $\mu = 0.07$ to 1.75. Two different rotor blade bending stiffness distributions and Lock numbers were included. As a result rotor response measurements were obtained for a total of approximately 40 test points having various combinations of these parameters.

Empirical Induced Inflow Model

The experimental data will first be used to obtain an empirical induced inflow model for comparison with the simple inflow theories presented previously. Equation (18) has been solved at each of the test points of the 7.5 ft model data. Since at each test point more response derivatives were measured than the nine unknown inflow derivatives of $[L]$ a least-squares method was used to find the best empirical inflow model at each test point. Each of the inflow derivatives was normalized by $a\sigma/\mu$ for comparison with the theoretical values of Eq. (21) and (24). The results of this procedure are shown in Fig. 4 with individual points for each inflow derivative plotted for each of the experimental test points. The line faired through these points will be referred to as the empirical inflow model.

At very low advance ratio $0 < \mu < 0.4$ most of the simple momentum and vortex theory inflow derivatives, Eqs. (21) and (24) are in qualitative agreement with the experimental data. Two of the derivatives, $d\lambda_0/d(C_T/a\sigma)$ and $d\lambda_c/d(C_T/a\sigma)$, are even in close quantitative agreement.

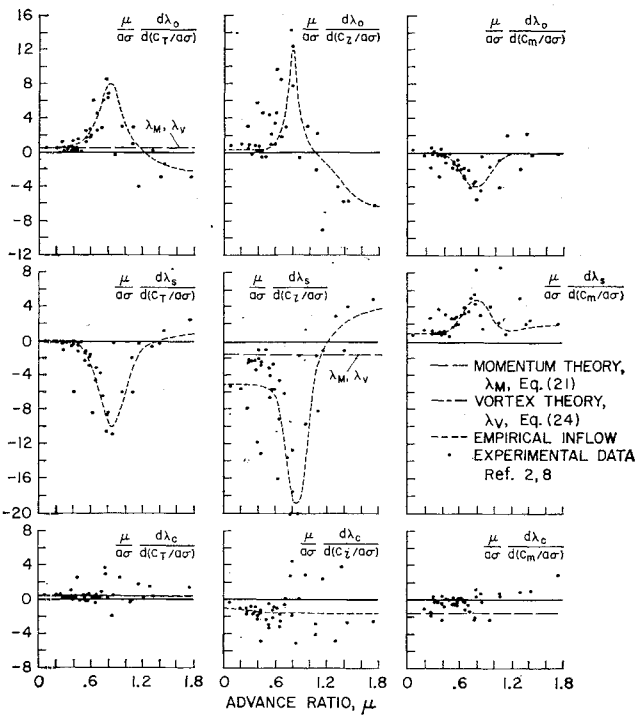

Fig. 4 Empirical nonuniform induced inflow model.

At higher advances ratios, six of the empirical inflow derivatives exhibit highly unusual behavior in the form of pronounced peaks centered around $\mu \simeq 0.8$. The consistency of these peaks suggests that the reversed flow region of the rotor may in some way exert a strong influence on the basic character of the induced velocity field of a hingeless rotor. At advance ratios near 0.8 the reversed flow region is large and the dynamic pressure relative to the rotor blade is greatly reduced. Thus the effective lifting area of the rotor disk is also correspondingly reduced. At higher advance ratios the reversed flow region is enlarged, but the dynamic pressure is no longer small and the full rotor disk area is aerodynamically effective. Therefore, for advance ratios near one, the reduction in effective rotor disk area would require higher loading per unit area and consequently increased induced inflow.

Since a significant degree of scattering is present in the experimental points of Fig. 4 some comment is warranted with regard to possible implications for the theoretical inflow model postulated by Eq. (13). First, however, it should be pointed out that considerable scattering could be expected from the influence of experimental error and inaccuracies of the generalized harmonic balance method. This is because the calculation of the inflow model is quite sensitive to relatively small differences between the theoretical (without inflow) and experimental response derivatives.

A more fundamental reason for the scattering could be related to the assumption, inherent in Eq. (13), that the inflow model is independent of rotor configuration parameters such as flap frequency (p), Lock number, and the flap bending mode shapes. These factors certainly influence the distribution of aerodynamic loading on the rotor, which uniquely determines the distribution of induced inflow. Therefore, it would be possible for two different rotors, generating the same total thrust and moments, to have different aerodynamic loading distributions and induced inflows. Although the present experimental data encompassed ten different values of flap frequency, no consistent trends were discernable in the empirical results. It is likely that analysis of additional experimental data will be required to establish the uniqueness

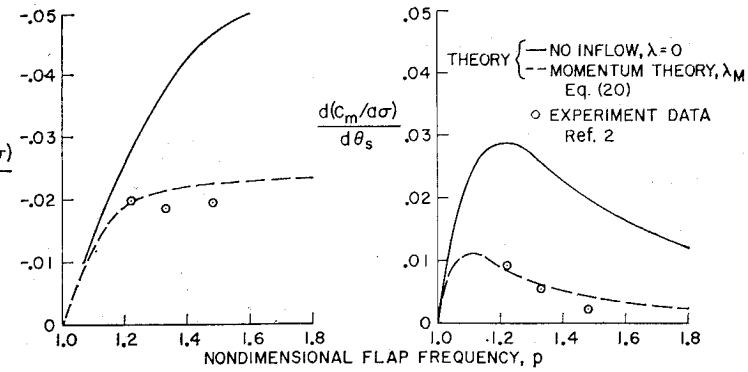

Fig. 5 Comparison of theory with 7.5-ft model data in hover, $C_T/\sigma = 0.012$, $\gamma = 5.0$, $B = 0.97$, $e_{pc} = 0.0$, $a\sigma = 0.729$, $e = 0.0$.

of the postulated inflow model with respect to configuration parameters.

Hover Condition

Correlation of theory and experiment for the hover condition is shown in Fig. 5. Theoretical pitch and roll moment response to longitudinal cyclic pitch is shown both with and without nonuniform inflow based on momentum theory, Eq. (20). Because of the insensitivity of the harmonic balance theory to rotor blade mode shape for $\mu = 0$, the results were computed for the simple rigid blade model without hinge offset, $e = 0.0$. The magnitude of the reduction in rotor control power, accentuated by the low value of mean inflow λ_o, is quite reasonably predicted by the simple momentum theory nonuniform inflow.

Low Advance Ratio Correlation

Selected rotor response derivatives using the various inflow models are compared with experimental data of Ref. 8 in Fig. 6 for the low advance ratio range. The theory without inflow is clearly inadequate and characteristically overestimates the measured results. Intuitively, this reflects the fact that the theory neglects the deflection of the airstream as it reacts to the forces and moments applied by the rotor.

The momentum theory inflow model, λ_m, Eq. (21) fairly consistently reduces the response derivatives, analogous to the hover results and significantly improves the correlation with the data. The inadequacies of the momentum inflow theory, however, are evident in comparison with several unusual features exhibited by the data, such as the reversal of $d(C_l/a\sigma)/d\theta_o$ and the magnification of $d(C_m/a\sigma)/d\theta_o$ at low advance ratio.

Shupe[4] proposed a convenient method of accounting for nonuniform inflow which defines an equivalent Lock number γ^*, derived on the basis of momentum theory, in terms of the actual Lock number

$$\gamma^* = \frac{\gamma}{1 + a\sigma/8\mu} \tag{25}$$

As shown in Fig. 6, the results are comparable to the momentum theory inflow model.

The vortex theory inflow model λ_v, Eq. (24), improves the qualitative behavior of response derivatives, particularly in connection with the discrepancies noted above for the momentum theory. This is almost entirely due to the nondiagonal inflow derivative $d\lambda_c/d(C_T/a\sigma)$ of Eq. (24). However, this derivative is unrealistic at very low μ because it produces a divergence in the $d(C_m/a\sigma)/d\theta_o$ response derivative.

Although the momentum and vortex theory inflow models reproduced nearly all of the characteristics of the measured data, their qualitative accuracy for the entire group of response derivatives is not adequate. Theoretical predictions

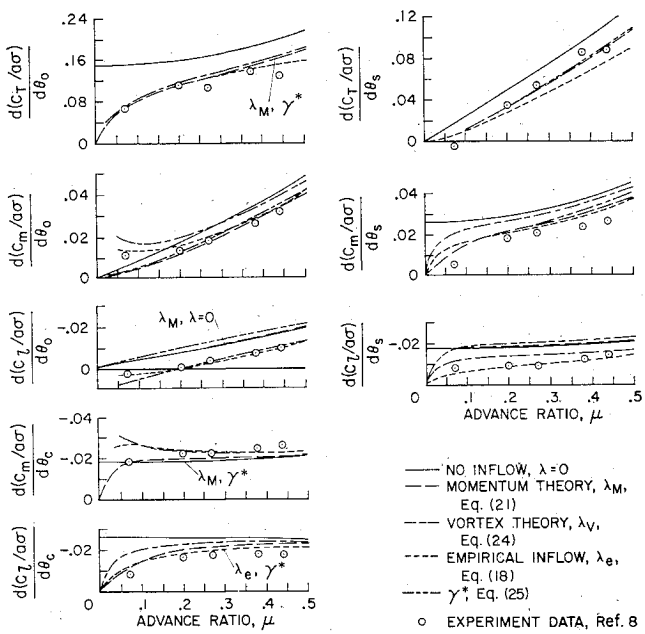

Fig. 6 Comparison of theory with 7.5-ft model data at low advance ratio, $C_T/a\sigma = 0.0$, $p = 1.17$, $\gamma = 4.2$, $B = 0.97$, $e_{pc} = 0.25$, $a\sigma = 0.729$, $J = 2$.

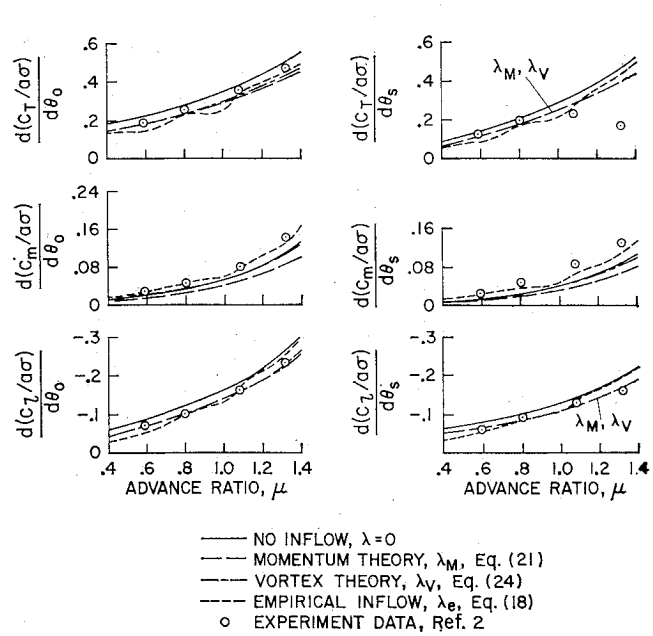

Fig. 7 Comparison of theory with 7.5-ft model data at high advance ratio, $C_T/a\sigma = 0.0$, $p = 2.32$, $\gamma = 4.2$, $B = 0.97$, $e_{pc} = 0.25$, $a\sigma = 0.729$, $J = 2$.

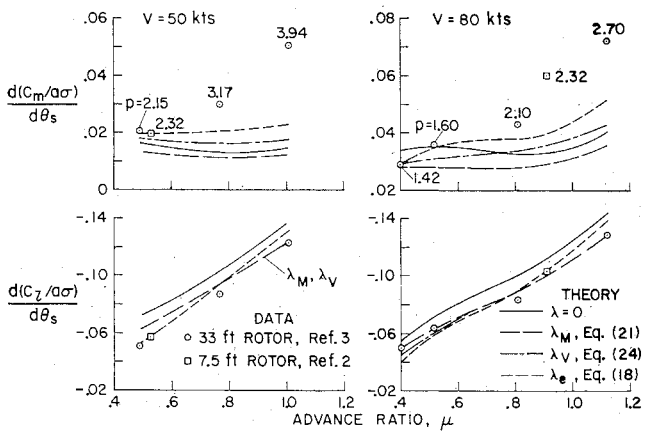

Fig. 8 Comparison of theory with 33-ft model data, $C_T/\sigma = 0.0$, $\gamma = 4.57$, $B = 0.97$, $e_{pc} = 0.0$, $a\sigma = 0.387$, $J = 2$.

using the empirical inflow model of Fig. 4 would be expected to give the best correlation, and are indeed a significant improvement over those using the purely theoretical inflow models. (The small discrepancies in this correltaion are due to the imperfect least squares solution for each data point in Fig. 4 and the deviations from the faired curve because of scattering).

High Advance Ratio Correlation

A second correlation is given in Fig. 7 for an advance ratio range which encompasses the region of the pronounced peaks observed in the empirical inflow derivatives. The experimental data, taken from Ref. 2, is qualitatively similar to the low advance ratio case except that some of the response derivatives substantially exceed the theoretical predictions without induced inflow. One reason for this may be the high value of flap frequency, $p = 2.32$, but also important is the effect of induced inflow at these high advance ratios. These effects render the simple momentum and vortex theories even more inadequate than the previous correlation at low advance ratio because of their tendency to diminish each of the theoretical response derivatives.

The empirical inflow model again yields an adequate correlation with the experimental data, however undesirable perturbations are present for advance ratios where the peaking occurs in the empirical inflow model. These perturbations could be reduced by refining the fairing of the peaks in the curves of the empirical inflow model in Fig. 4.

Large-Scale Model Correlation

It is of interest to apply the methods developed for the study of the small scale rotor model data to experimental results obtained with a large scale hingeless rotor model. Reference 3 contains data for a 33-ft-diam model and selected results are correlated with the present theories in Fig. 8. The advance ratio of the test data was changed by varying rotor angular velocity which also changed the rotor blade flap frequency. The resulting value of p is noted beside each data point.

The theory without inflow is shown to be inadequate as in the previous correlations, but the discrepancy becomes particularly pronounced for the pitching moment response at high advance ratio. The various inflow theories are shown to improve the correlation especially for the roll moment response. The empirical inflow obtained from the 7.5-ft-model rotor data provides the best correlation, however, a large discrepancy remains for the pitching moment response at the high advance ratio points. A possible explanation is the extremely large value of flap frequency. If it is true that this is the significant factor, then it could imply that the empirical inflow model is not independent of configuration parameters as discussed above.

Conclusions

1) For very low μ or high p, the simple approximations for the first flap bending mode give accurate results. But for moderate values of μ and p, the first two elastic flap modes must be used to accurately predict hingeless rotor response.

2) The effects of induced inflow are important for both low and high advance ratios. The simple vortex theory gave nearly adequate correlation with measured response data.

3) The empirical inflow model presented above can be used to obtain the best prediction of hingeless rotor response, but its sensitivity to rotor configuration parameters remains to be established.

4) The empirical inflow model revealed large unexpected variations in the induced inflow characteristics of the rotor for advance ratios near 0.8.

References

[1] Sissingh, G. J., "Dynamics of Rotors Operating at High Advance Ratios," *Journal of the American Helicopter Society*, Vol. 13, No. 3, July 1968, pp. 56–63.

[2] Kuczynski, W. A. and Sissingh, G. J., "Research Program to Determine Rotor Response Characteristics at High Advance Ratios," CR 114290, Feb. 1971, NASA.

[3] Watts, G. A., London, R. J., and Snoddy, R. J., "Trim, Control and Stability of a Gyro-Stabilized Hingeless Rotor at High Advance Ratio and Low Rotor Speed," CR-114362, May 1971, NASA.

[4] Shupe, N. K., "A Study of the Dynamic Motions of Hingeless Rotored Helicopters," PhD. thesis, 1970, Princeton Univ.

[5] Bisplinghoff, R. L., Ashley, H., and Halfman, R. L., *Aeroelasticity*, Addison-Wesley, Reading, Mass., 1955.

[6] Yntema, R. T., "Simplified Procedures and Charts for the Rapid Estimation of Bending Frequencies of Rotating Beams," TN 3459, June 1955, NACA.

[7] Stepniewski, W. Z., *Introduction to Helicopter Aerodynamics*, Rotorcraft Publishing Committee, 1958.

[8] Kuczynski, W. A. and Sissingh, G. J., "Characteristics of Hingeless Rotors With Hub Moment Feedback Controls Including Experimental Rotor Frequency Response," Vol. I, CR-114427, Jan. 1972, NASA.